Generation of Multiple Excitons in Ag2S Quantum Dots: Single High-Energy versus Multiple-Photon Excitation

ARTICLE *in* JOURNAL OF PHYSICAL CHEMISTRY LETTERS · JANUARY 2014

Impact Factor: 7.46 · DOI: 10.1021/jz5000512

8 AUTHORS, INCLUDING:

Weili Yu
King Abdullah University of Science and Tec…
26 PUBLICATIONS **432** CITATIONS
SEE PROFILE

Tayirjan T. Isimjan
King Abdullah University of Science and Tec…
6 PUBLICATIONS **50** CITATIONS
SEE PROFILE

Erkki Alarousu
King Abdullah University of Science and Tec…
71 PUBLICATIONS **496** CITATIONS
SEE PROFILE

Kazuhiro Takanabe
King Abdullah University of Science and Tec…
126 PUBLICATIONS **4,437** CITATIONS
SEE PROFILE

THE JOURNAL OF PHYSICAL CHEMISTRY Letters

Letter

pubs.acs.org/JPCL

Generation of Multiple Excitons in Ag_2S Quantum Dots: Single High-Energy versus Multiple-Photon Excitation

Jingya Sun,[†,§] Weili Yu,[‡,§] Anwar Usman,[†] Tayirjan T. Isimjan,[†] Silvano DGobbo,[†] Erkki Alarousu,[†] Kazuhiro Takanabe,[‡] and Omar F. Mohammed*[,†]

[†]Solar and Photovoltaic Engineering Research Center and [‡]KAUST Catalysis Center, Division of Physical Sciences and Engineering, King Abdullah University of Science and Technology, Thuwal 23955-6900, Saudi Arabia

Supporting Information

ABSTRACT: We explored biexciton generation via carrier multiplication (or multiple-exciton generation) by high-energy photons and by multiple-photon absorption in Ag_2S quantum dots (QDs) using femtosecond broad-band transient absorption spectroscopy. Irrespective of the size of the QDs and how the multiple excitons are generated in the Ag_2S QDs, two distinct characteristic time constants of 9.6−10.2 and 135−175 ps are obtained for the nonradiative Auger recombination of the multiple excitons, indicating the existence of two binding excitons, namely, tightly bound and weakly bound excitons. More importantly, the lifetimes of multiple excitons in Ag_2S QDs were about 1 and 2 orders of magnitude longer than those of comparable size PbS QDs and single-walled carbon nanotubes, respectively. This result is significant because it suggests that by utilizing an appropriate electron acceptor, there is a higher possibility to extract multiple electron−hole pairs in Ag_2S QDs, which should improve the performance of QD-based solar cell devices.

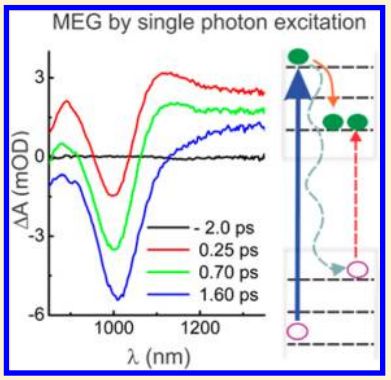

SECTION: Kinetics and Dynamics

Flexible solar panels made from semiconductor quantum dots (QDs) have great potential to be useful light-harvesting materials, opening up an optimistic view to utilize this new technology in third-generation photovoltaic devices.[1−3] The advantages of QD-sensitized solar cells are their adjustable band gap energy through the control of the size of the QDs,[4] their high extinction coefficient,[5] and their shape, composition, and low cost.[2,3] Typically, in semiconductors, a single high-photon absorption creates one charge carrier, and when the photon energy of the excitation beam is higher than the band gap energy (E_g), the excess energy is dissipated through electron−phonon interactions,[6] or it can be transferred via the Coulomb interaction to the valence band to create one or more additional electron−hole (e−h) pairs.[7−9] The formation of two or more excitons for the cost of one absorbed photon is called multiple-exciton generation (MEG), which is carrier multiplication due to impact ionization in bulk semiconductors.[9−12] The possibility of optimizing MEG for efficient photon-to-current solar energy conversion has been evaluated by several groups using a variety of QDs, including PbS,[13,14] PbSe,[13,15−17] CdSe,[18] InAs,[19] and Si,[20] and single-walled carbon nanotubes.[21] More recently, MEG in the photocurrent of QD-based solar cell exhibits an external quantum efficiency (the spectrally resolved ratio of collected charge carriers to incident photons) of 114% with the threshold at $2.6E_g$.[17] The use of MEG for solar energy applications has been reviewed by Beard et al.[22]

The energy threshold required to generate MEG decreases drastically from bulk semiconductors to QDs.[14] Although the reason for the decrease in the MEG threshold is still being debated in the literature, it is generally discussed in terms of an increase in the Coulomb interaction, that is, the smaller density of states would tend to decrease the MEG rate.[23] Another possibility that is often discussed is the reduced cooling rate caused by the sparse density of states.[24] In some cases, the threshold photon energy of MEG in QDs can be significantly reduced to approach twice the band gap energy.[25] For PbS QDs, the MEG threshold is size-dependent, and in PbS QDs with band gaps smaller than 900 nm, the threshold can be as close as the theoretical energy conservation limit of $2E_g$.[14] Interestingly, a very high MEG quantum yield (QY) of 700% (using excitation with photon energy at $7.8E_g$) has been reported for PbSe QDs,[25] but this value was considered to be overestimated due to photoionization in the presence of multiple excitons.[14,26] On the other hand, a typical range of 200−300% for other QDs depending upon the excess energy of $3−4E_g$ of the absorbed photon was measured.[13,15,18,20,27] In sharp contrast, a very low or even the absence of the MEG process in similar QDs has also been reported.[26,28,29] With the dynamic spectroscopic condition and careful spectroscopic analysis on MEG by single photons, the MEG data in ref 27 have been established and are reproducible.[30]

Several theoretical and experimental investigations have also been devoted to the fundamental mechanism for understanding

Received: January 8, 2014
Accepted: January 28, 2014

   dx.doi.org/10.1021/jz5000512 | J. Phys. Chem. Lett. 2014, 5, 659−665

and finally controlling the MEG process in many semiconductor QDs.[11,17,31−36] As an advance in this area, we propose the use of Ag_2S QDs as a new material system for MEG and solar cells applications because they have very high photostability, low toxicity, and low threshold photon energy for electron multiplication and long lifetimes of the generated multiple e−h pairs. Moreover, they are considered to be a convenient model system for strongly confined MEG study[37] due to their tunable E_g in the near-infrared (IR) region,[38,39] their bright photoluminescence, their highly monodispersed colloids,[40] their high photostability,[41,42] and their suitability for optimizing photovoltaic devices.[43]

Another practical way to generate multiple excitons in QDs is to photoexcite them with high pump fluence.[44] In this case, the QDs absorb more than one photon, generating more than a single exciton per QD. The presence of multiple excitons in QDs, no matter whether they are generated by one or several photon(s), is usually indicated by their distinct nonradiative Auger recombination. In this case, a fast e−h recombination is typically observed, leaving only one exciton per individual QD, which is governed by a slow radiative decay due to e−h recombination. Thus, by analyzing the relative contributions of fast and slow components, the MEG threshold and the quantum efficiency can be directly determined.[15,24] Among time-resolved spectroscopic techniques, the best technique to monitor the MEG process is transient absorption (TA) spectroscopy with broad-band capability that allows a broad spectral range to be covered even in the near-IR, where the first exciton absorption peak is located.[24]

In this Letter, we report the carrier dynamics and MEG efficiency in Ag_2S QDs with band gaps in the range of 1.55−1.07 eV using femtosecond TA spectroscopy with broad-band capability. The time-resolved data clearly show the existence of two binding strengths of e−h pairs regardless of the method of generation (single- or multiple-photon excitation), namely, tightly bound and weakly bound excitons, and they can be distinguished by the distance of the charge carrier from the hole. Moreover, the ratio between the two types of multiple excitons can be controlled by the solvent polarity, pump fluence, and QD size as well. In addition to this observation, we found that the threshold photon energy for MEG of Ag_2S QDs with the band gap of 1.23 eV is $2.28E_g$, with a quantum efficiency of 173% per single-absorbed photon at a pump photoexcitation of 3.2 times the band gap.

In Figure 1A, we show representatively a high-resolution transmission electron microscope (HRTEM) image of a single Ag_2S QD (with a ∼9.0 nm diameter), the size distribution, and the steady-state absorption spectrum. As can be seen, the size distribution is quite narrow like other semiconductors QDs.[45] We assigned the absorption peak centered at 1010 nm to the lowest optical transition between spatially confined electron and hole states (band gap, E_g). The TA spectra obtained by probing with white light tuned to the first excitonic absorption peak after the 830 nm ($1.2E_g$) excitation are also shown in Figure 1B−E. As can be clearly seen, the transient spectra depend strongly on the applied pump fluence (from 0.15 to 2.29 mJ/cm^2; corresponding to 6.38×10^{14} to 9.57×10^{15} photons/cm^2). At a low fluence of ∼0.15 mJ/cm^2 (Figure 1B), the ground-state bleach (GSB) shows almost no recovery on the picosecond time scale. The absence of the fast component of GSB recovery at such low pump fluence indicates that the photoexcitation generates a single exciton that has a lifetime that is much longer than the observation window, and we

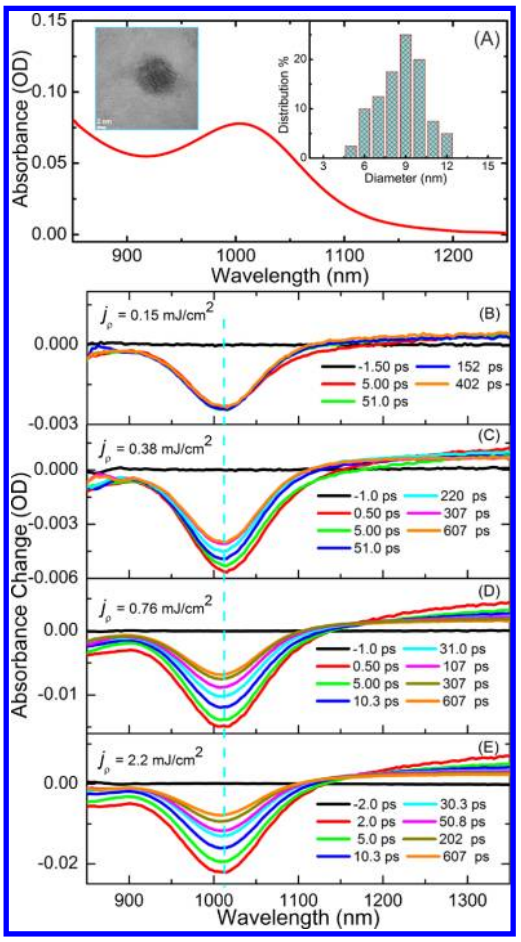

Figure 1. (A) The steady-state absorption spectrum of Ag_2S QDs with a peak absorption maximum corresponding to the first exciton ($1S_h$−$1S_e$ transition) at 1010 nm in ethylene glycol. (Inset) A high-resolution TEM image of a single QD with a 2 nm scale bar, and the size distributions of Ag_2S-1010. (B−E) TA spectra at time delays from 0.5 to 607 ps under different laser fluences of 830 nm ($1.2E_g$) light excitation.

consider the relevant dynamics of the single exciton as a reference or benchmark to evaluate the multicarriers formation. As shown in Figure 1C−E, when we increased the pump fluence, we observed a clear acceleration of the bleach decay and increases in the percentage of its recovery due to Auger recombination processes of multiple e−h pairs. The TA data show two fast components of GSB recovery on the tens and hundreds of picosecond time scale (see also Figure 2). Because the excitons occupy the electronically cold state (the band edge) of the conduction band, we did not observe excitons with excess energy (hot excitons). In this regime, the single exciton shows a very long lifetime, as demonstrated by the low pump fluence. Subsequently, the fast components of the carrier dynamics at the high pump fluence can be attributed to multicarriers produced by multiple-photon absorption.[21]

To demonstrate the critical influence of the confinement on the dynamics of Auger recombination of multiple e−h pairs in Ag_2S QDs, we also analyzed a smaller Ag_2S QD with a band gap energy of 1.55 eV. As indicated in Figure 3B, after excitation with the photon energy at $1.2E_g$, the Auger recombination dynamics of multiple excitons shortened from 10.5 and 185 ps with a band gap of 1010 nm (1.24 eV) to 5.5 and 159 ps with a band gap of 800 nm (1.55 eV). Being in this regime, we also

dx.doi.org/10.1021/jz5000512 | J. Phys. Chem. Lett. 2014, 5, 659−665

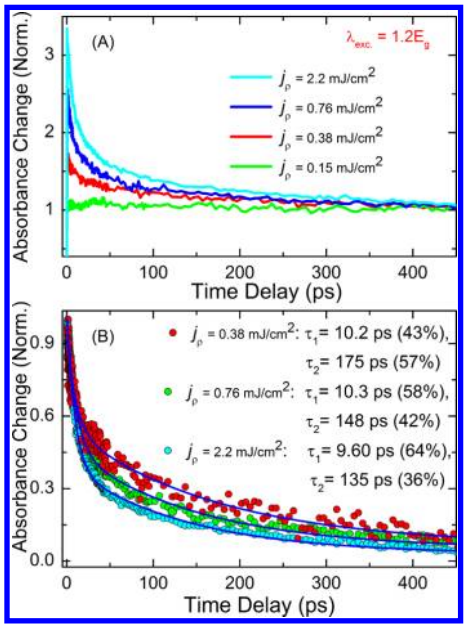

Figure 2. (A) The kinetics of different absorptions at the ground bleach peak (1010 nm) under different pump fluences. (B) Comparison of the kinetics of multiple excitons. The lines are the best fits with two exponential decay functions.

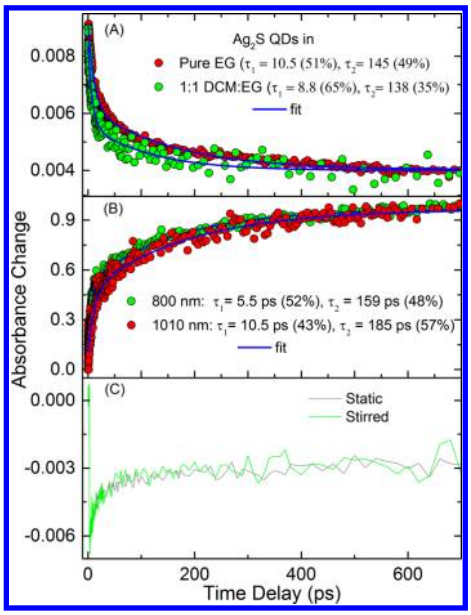

Figure 3. (A) The kinetics of the GSB recovery in different polarities of the solvent medium. (B) The bleach of the first exciton state for Ag_2S-800 (green) and Ag_2S-1010 (red) under the photoexcitation with a photon energy of $1.2E_g$. (C) The GSB recovery for stirred and static colloidal QDs dispersed in ethylene glycol.

found that the Auger recombination time constants increase with the decrease in the band gap. In other words, our results reveal systematic scaling of the carrier recombination time constants with QD volume (see Figure S2, Supporting Information). This result demonstrates that the exciton depopulation should be attributed to Auger recombination.

To evaluate the relaxation dynamics of multicarriers, in Figure 2A, we show the kinetics of the GSB recovery at 1010 nm. The GSB recovery increased with increasing excitation fluence. Because the GSB is due to the $1S_h \rightarrow 1S_e$ transition and it is directly associated with the population of excitons, the results indicate that the number of e−h pairs (the multicarriers) increases significantly by increasing the pump fluence. As shown in Figure 2B, the decay of the multicarriers is estimated by fitting the kinetic data with a two-exponential decay function instead of the single-exponential decay found in PbS,[14] PbSe,[15] and CdSe.[27] The fit gives two characteristic time constants, τ_1 = 9.6−10.3 ps and τ_2 = 135−175 ps, depending on the excitation fluence in the range of 0.38−2.2 mJ/cm^2. The increase of the pump intensity not only changes the ratio between the two components but also shortens the time constants of the nonradiative Auger recombination, indicating that the carrier dynamics (Auger recombination) becomes faster as the number of e−h pairs increases. This is not surprising because multiple e−h pairs lead to an increase in the Auger-accelerated multiple-exciton recombination. It is worth mentioning that the sample follows the Poisson statistics, as described below. As shown in Figure 2B (also see Figure S4, Supporting Information), this suggests that the highest pump intensity in this work is still below the saturation fluence to generate multicarriers. From the two relaxation time constants, it is clear that the generated multicarriers undergo two recombination processes, leaving finally a long-lived single exciton. Considering that Auger recombination in QDs is due to enhanced Coulomb interactions and relaxation of momentum conservation,[44] the two components of the relaxation dynamics reflect the nonradiative Auger recombination of the multicarriers. The existence of two or more excitons within one QD produces an efficient Auger biexciton recombination, that is, an exciton recombines via energy transfer and/or the other exciton is excited into a higher-energy state and then decays into the edge of the conduction band through intraband relaxation.[15,24,34,46,47] In this regard, the two time constants can be explained by Auger biexciton recombination of two types of excitons in Ag_2S QDs that are related to the distinct distance charge carrier from the hole as well as to the distinct strength of the Coulomb interaction, as observed in many semiconductors.[46,48] This means that the second decay component is attributed to a different type of biexciton rather than a triexciton. Although it is reasonable to consider that the photoexcitation above the saturation fluence can possibly create triexcitons, the absence of the triexcitons is also supported by the observation of the second decay component at a low fluence of the photon energy at $3.2E_g$, as described below. Because Ag_2S is a monodispersed colloid, the characteristic time constants, τ_1 and τ_2, can therefore be attributed to Auger recombination of different locations of the electron and hole, or more precisely due to different binding excitons. In this case, the relaxation decay of weakly bound excitons (the slow component) is about 1 order of magnitude slower than that of tightly bound excitons. As proposed by Nozik for the different types of excitons in QDs, the tightly bound exciton in both the electron and hole remains in the QD core and is energetically easier to recombine, whereas the weakly bound exciton is a charge-separated one with the hole at the QD surface.[46]

It is worth pointing out that the polarity of the ethylene glycol, the solvent, may facilitate such a charge separation at the QD surface. By directly comparing the kinetics at different excitation fluences (Figure 2B), we found that the population of tightly bound excitons increases as the pump fluence increases, indicating that multiple excitons in single QDs can affect the distance of the charge carrier from the hole and, thus, the strength of their Coulomb interactions. On the basis of the high

dx.doi.org/10.1021/jz5000512 | J. Phys. Chem. Lett. 2014, 5, 659−665

photostability (see Figure 3C) of Ag_2S QDs and the constantly stirred solution using a magnetic stirrer such that a fresh sample was available for each laser shot, we can exclude any contribution to the measured signal from the photocharging.

To verify the validity of the existence of two binding excitons experimentally, we exchanged the dielectric constant of the medium from pure ethylene glycol to a dichloromethane/ethylene glycol (1:1) mixture. Because the localization length of the excitons is affected by macroscopic polarization,[49] which is linearly correlated with the dielectric constant, we expected that the population of the tightly bound exciton will be higher as compared with that of the weakly bound exciton in a less polar medium, which is what we observed in the dichloromethane/ethylene glycol mixture. As shown in Figure 3, the kinetics of the two relaxation pathways tends to be faster in media with lower dielectric constants. Importantly, the amplitudes of the two components indicate that the tightly and weakly bound excitons are comparable with each other in the high polarity of the solvent, whereas the tightly bound excitons are higher in the lower polar solvent as the exciton binding energy increases. This result is consistent with the fact that the polarity of the ethylene glycol may facilitate the charge separation at the QD surface and subsequently increase the amplitude of the weakly bound excitons. This observation supports the existence of the two binding excitons.

The average number of photons absorbed per QD follows Poisson statistics such that $N_{abs} = j_p\sigma$, where j_p is the pump fluence and σ is the absorption cross section of Ag_2S QDs at the pump wavelength. The value of $\sigma = 0.25 \times 10^{-15}$ cm^2 is determined from the absorption coefficient of QDs at the excitation photon energy. The average population of excitons ($\langle N_{e-h}\rangle$) was obtained by dividing the initial TA signal amplitude (multiexcitons) by the long-time signal (single exciton); see also Figure S3 (Supporting Information). On the other hand, at a pump fluence as low as $j_p = 0.15$ mJ/cm^2, N_{abs} is calculated to be 0.164. At this condition, the generation of multicarriers by multiphoton absorption is not expected to occur as supported by the absence of the fast component of GSB recovery (see Figure 1B). As a result, the lowest pump fluence is set to $\langle N_{e-h}\rangle = 1$. Being in this regime, the blue solid line in Figures 4 and S4 (Supporting Information) is the linear fit to $\langle N_{e-h}\rangle$ (which is extracted from the GSB recovery signal) only at low pump fluence. This indicates that $\langle N_{e-h}\rangle$ and, hence, the efficiency of the multicarrier formation are most likely determined by Poissonian distribution. Accordingly, the Poisson distribution, the probability of generating $\langle N_{e-h}\rangle$ due to absorbing two or more photons is dictated by the factor $[(1 - \exp(-N_{abs}))/N_{abs}]$; thus, it is reasonably higher with j_p, but it tends to saturate at high pump fluences (see Figure 4).

To understand the MEG induced by a single photon with an excess energy, in Figure 5A,B, we show the time-resolved spectra at early time delays after excitation at 830 and 315 nm (equivalent to $1.2E_g$ and $3.2E_g$, respectively) with a pump fluence of ~0.15 mJ/cm^2. As can be clearly seen, the exciton with an excess energy induces featureless absorption spectra across the whole observation window and a blue shift of the GSB (~10 nm). These results indicate that the hot exciton relaxation and MEG process take place very rapidly within a couple of hundred femtoseconds. Figure 6A shows that there is no fast recombination of the exciton at the excitation energy of $1.2E_g$ because N_{abs} is less than 0.2 at this level of pump fluence. By normalizing the GSB recovery of the exciton at time delays longer than 600 ps (Figure 6C), additional fast components are

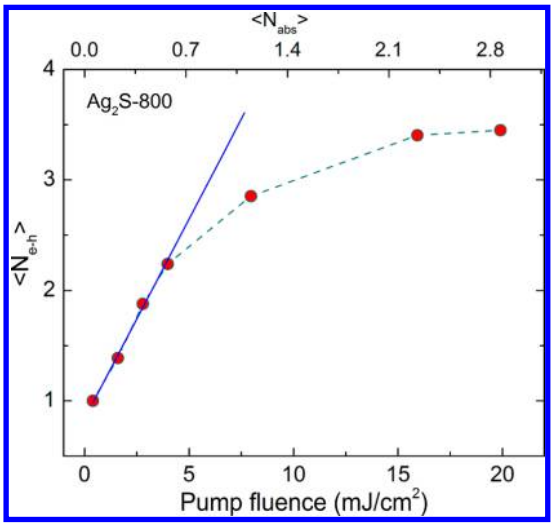

Figure 4. The average population of excitons (N_{e-h}) in Ag_2S-800 QDs as a function of pump fluence and the number of absorbed photons per QD. The solid line indicates the linear dependence of the exciton population at low pump fluences.

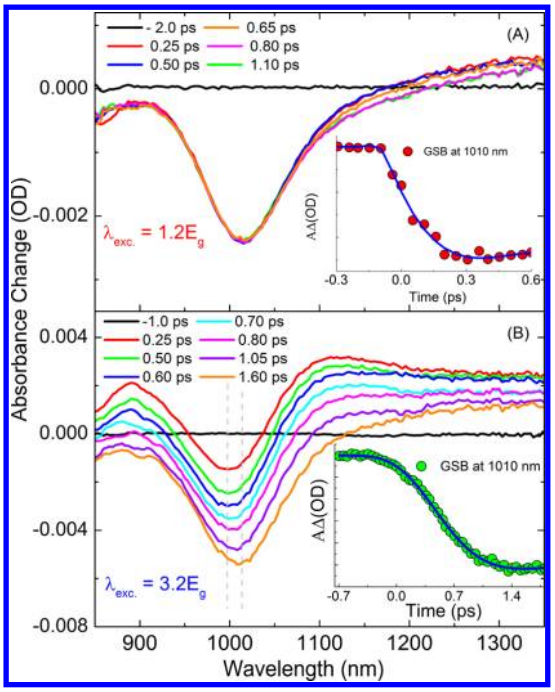

Figure 5. TA spectra of Ag_2S QD_S at early time delays after $1.2E_g$ (A) and $3.2E_g$ (B) excitation with the number of photons per QDs less than 0.20. (Inset) The formation of the multiple excitons by multiphoton (A) and by single high-energy photon (B) absorption, showing the hot electron formation and relaxation in the case of single high-energy photon excitation.

clearly observed under the 315 nm excitation conditions ($3.2E_g$) compared to that under 830 nm excitation conditions ($1.2E_g$). It is worth pointing out that the GSB recovery at the excitation with a pump energy of $3.2E_g$ (with 0.15 mJ/cm^2 pump fluence) is similar to that at $1.2E_g$ (0.38 mJ/cm^2), an excitation with multiple photons (see Figure 2A). Moreover, the two exponential decay components of the exciton relaxation are also consistent with each other, suggesting that the excitation with a single photon of $3.2E_g$ also generates multiple e−h pairs. It should be noted that we found that the

dx.doi.org/10.1021/jz5000512 | J. Phys. Chem. Lett. 2014, 5, 659−665

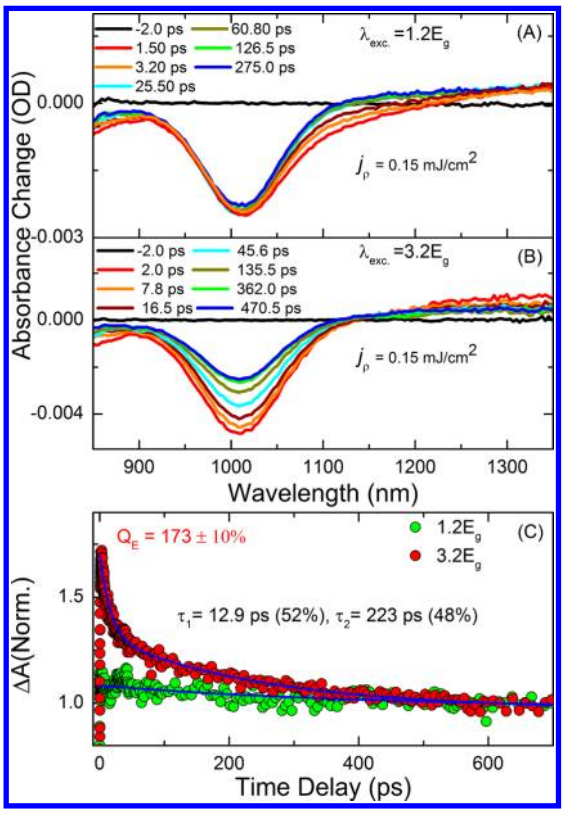

Figure 6. TA spectra of the GSB at 1010 nm after excitation with pump energies of $1.2E_g$ (A) and $3.2E_g$ (B) with a laser fluence of 0.15 mJ/cm^2. (C) The bleach of the first exciton state for Ag_2S-1010 at photon energies of $1.2E_g$ (green) and $3.2E_g$ (red). By dividing the initial TA signal amplitude (multiexciton) by the long-time signal (single exciton), the photoexcitation quantum efficiencies of Ag_2S QDs were calculated. Note that the sign of the signal is reversed and normalized for clarity.

characteristic time constants of the MEG due to the multiple-photon absorption are slightly faster than those generated by a single high-energy photon. Although the difference is reproducible, the origin of such a difference cannot be explained by our experimental data, and one may turn to high-level theoretical investigations that are beyond the scope of this study.

At the low fluences, the MEG QY can be determined from the ratio between the initial signal amplitude of multiple excitons (ΔA_{me}) and the long-time signal amplitude single exciton (ΔA_{se}).[14,50] For accuracy of MEG estimation, the direct generation of multiple excitons via absorption of multiple photons has been corrected based on Poisson distribution of photon absorption events. Under our experimental conditions, the Poisson distribution factor $[(1 - \exp(-N_{abs}))/N_{abs}]$ is 0.922, and thus, the MEG QY is calculated as QY = $0.922(\Delta A_{me}/\Delta A_{se})$.[50]

Figure 7 shows the MEG QY measured at different excitation wavelengths, where the extracted MEG threshold photon energy was $\sim 2.28E_g$. For photon excitation energies of $2.5E_g$ and $3.2E_g$, the MEG QYs were measured to be 118 and 173%, respectively. We also measured the Auger recombination at lower and lower fluence for the case of the $3.2E_g$ excitation and found within our experimental sensitivity that the carrier dynamics are independent of the fluence (see Figure S5, Supporting Information), providing clear evidence that the multiple excitons are generated by a single high-energy photon

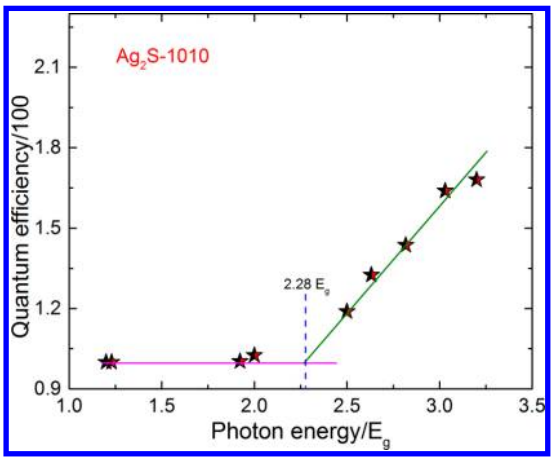

Figure 7. A plot of the MEG QY as a function of the pump energy for Ag_2S-1010 by which the MEG threshold is estimated to be $2.28E_g$.

rather than multiphoton absorption process. In addition, when we diluted the sample by a factor of 5 and adjusted the pump fluence to get the same number of absorbed photons per QDs, similar dynamics for carrier recombination is observed, indicating that our estimation for the MEG QY is quite valid under these experimental conditions. Our results are comparable with a recently published MEG in PbS QDs and single-walled carbon nanotubes with similar E_g. For instance, The MEG QY was 174% at the excitation energy of $3E_g$ for PbS-880,[51] and it was about 130% at the excitation energy of $2.5E_g$ for the single-walled carbon nanotube[21] and for PbS-930.[14] It is noteworthy that the τ_2 of the relaxation decay of MEG in Ag_2S QDs was about 1 and 2 orders of magnitude longer than that of the comparable size PbS (<20 ps)[14,51] and the single-walled carbon nanotube (~1 ps),[21] respectively. This comparison is significant because it indicates that, via use of an appropriate electron acceptor, multiple e−h pairs in Ag_2S QDs has greater possibility to be extracted and subsequently to improve the performance of a Ag_2S-based solar cell device. Because the weakly bound excitons in Ag_2S QDs have a 10 times longer population time than the tightly bound excitons, it is also interesting to note that in the ensemble electron donor and acceptor in the solar cell device, the weakly bound excitons are ideal for optical gain, charge separation, and so forth.[52,53]

In conclusion, we measured the carrier dynamics and MEG in Ag_2S QDs using femtosecond broad-band TA spectroscopy. We found that multiple excitons in the QDs can be generated either by multiphoton excitation at high pump fluence or by single high-energy photon excitation. Irrespective how the multiple excitons are generated in the Ag_2S QDs, the existence of two relaxation decays of the Auger recombination are evident, indicating the existence of two binding excitons, a tightly bound exciton and a weakly bound exciton. With single-photon excitation, the MEG efficiency is 173% (under an excitation energy of $3.2E_g$), and the MEG threshold is $2.28E_g$, suggesting that the MEG process in Ag_2S QDs has a threshold photon energy close to the theoretical energy conservation limit.

METHODS

Ag_2S QDs Synthesis. The QDs were grown using a solution-based route as described in an earlier report.[54] In brief, 3-mercaptopropionic acid and silver nitrate ($AgNO_3$) with a molar ratio of 2:1 were dissolved in ethylene glycol (50 mL).

dx.doi.org/10.1021/jz5000512 | J. Phys. Chem. Lett. 2014, 5, 659−665

After stirring and bubbling with argon at 110 °C for 30 min, the temperature was increased to 150 °C and maintained to allow the QDs to grow. When the solution changed from cloudy yellow to clear, aliquots of the solution were extracted at intervals of 2 min. The aliquots were collected in a set of glass vials to monitor the growth by optical characterization. During the growth process, a noticeable color change from light yellow to brown was detected, indicating that the size of the nanocrystals was increasing. The solution was then cooled down to room temperature, and 3-mercaptopropionic acid-coated Ag_2S QDs were obtained and used for TA measurements. The dynamics of the photoexcited carriers and MEG of the Ag_2S QDs were investigated by broad-band TA spectroscopy with a 120 fs time resolution, as described below. We carefully performed the multicarrier measurements in Ag_2S QDs at different pump fluences of light excitation at $1.2E_g$ to investigate how the multicarrier formation depends on the incident number of photons. Careful analysis of the recovery dynamics of the GSB was also performed for different pump photon energies ($1.2-3.2E_g$) to investigate the MEG threshold and efficiency in Ag_2S QDs. For comparison, we analyzed carrier dynamics and MEG efficiency in different sizes of Ag_2S QDs and with different polarities of the solvent medium.

TA Spectroscopy. The time-resolved pump−probe spectroscopy with broad-band capability was previously reported in detail.[51] Briefly, a few μJ of pulse energy as the fundamental output from a Ti:Sapphire femtosecond regenerative amplifier (800 nm, 35 fs fwhm, 1 kHz) was used to generate pump and probe beams. By introducing the fundamental beams into an optical parametric amplifier (Newport Spectra-Physics), we could select a certain wavelength from the tunable output (240−2600 nm) as the pump pulses, whereas light continuum probe pulses were obtained by focusing the fundamental beams onto a 2-mm-thick sapphire plate (contained in an Ultrafast System LLC spectrometer). The pump and probe pulses overlapped by a small angle of less than 5° in a 2-mm-thick cuvette cell containing Ag_2S QDs dispersed in ethylene glycol. The optical density of the sample at the excitation wavelength was less than 0.06 in a 2 mm quartz cell. The transmitted probe light from the samples was collected and focused on the broad-band IR detector for recording the time-resolved excitation-induced difference spectrum (ΔA). During the measurements, the solution was constantly stirred using a magnetic stirrer such that a fresh sample was available for each laser shot as well as to avoid photocharging of the QDs.

■ ASSOCIATED CONTENT

Supporting Information

Descriptions of the schematic diagram of the transient absorption spectroscopy system, absorption spectra of Ag_2S QDs, a plot of the lifetime of the biexciton versus QD volume, the kinetics of the ground bleach recovery at 800 nm under different pump fluences, average population of excitons in Ag_2S-1010 QDs as a function of pump fluence, and a plot of the number of electron−hole pairs at different pump fluences for the case of $3.2E_g$ excitation. This material is available free of charge via the Internet at http://pubs.acs.org.

■ AUTHOR INFORMATION

Corresponding Author

*E-mail: omar.abdelsaboor@kaust.edu.sa, omar3070@caltech.edu (O.F.M.).

Author Contributions

[§]J.S. and W.Y. contributed equally to the work.

Notes

The authors declare no competing financial interest.

■ REFERENCES

(1) Nozik, A. J. Quantum Dot Solar Cells. *Phys. E* **2002**, *14*, 115−120.
(2) Kamat, P. V.; Tvrdy, K.; Baker, D. R.; Radich, J. G. Beyond Photovoltaics: Semiconductor Nanoarchitectures for Liquid-Junction Solar Cells. *Chem. Rev.* **2010**, *110*, 6664−6688.
(3) Kamat, P. V. Quantum Dot Solar Cells. The Next Big Thing in Photovoltaics. *J. Phys. Chem. Lett.* **2013**, *4*, 908−918.
(4) Yu, W. W.; Qu, L.; Guo, W.; Peng, X. Experimental Determination of the Extinction Coefficient of CdTe, CdSe, and CdS Nanocrystals. *Chem. Mater.* **2003**, *15*, 2854−2860.
(5) Kamat, P. V. Quantum Dot Solar Cells. Semiconductor Nanocrystals as Light Harvesters. *J. Phys. Chem. Lett. C* **2008**, *112*, 18737−18753.
(6) Shockley, W.; Queisser, H. J. Detailed Balance Limit of Efficiency of pn Junction Solar Cells. *J. Appl. Phys.* **1961**, *32*, 510−519.
(7) Kolodinski, S.; Werner, J. H.; Wittchen, T.; Queisser, H. J. Quantum Efficiencies Exceeding Unity Due to Impact Ionization in Silicon Solar Cells. *Appl. Phys. Lett.* **1993**, *63*, 2405−2407.
(8) Wolf, M.; Brendel, R.; Werner, J. H.; Queisser, H. J. Solar Cell Efficiency and Carrier Multiplication in $Si_{1-x}Ge_x$ Alloys. *J. Appl. Phys.* **1998**, *83*, 4213−4221.
(9) Landsberg, P. T. *Recombination in Semiconductors*; Cambridge University Press: Cambridge, U.K., 1991.
(10) Schaller, R. D.; Agranovich, V. M.; Klimov, V. I. High-Efficiency Carrier Multiplication through Direct Photogeneration of Multi-Excitons via Virtual Single-Exciton States. *Nat. Phys.* **2005**, *1*, 189−194.
(11) Pijpers, J. J. H.; Ulbricht, R.; Tielrooij, K. J.; Osherov, A.; Golan, T.; Delerue, C.; Allan, G.; Bonn, M. Assessment of Carrier-Multiplication Efficiency in Bulk PbSe and PbS. *Nat. Phys.* **2009**, *5*, 811−814.
(12) Stewart, J. T.; Padilha, L. A.; Bae, W. K.; Koh, W.-K.; Pietryga, J. M.; Klimov, V. I. Carrier Multiplication in Quantum Dots within the Framework of Two Competing Energy Relaxation Mechanisms. *J. Phys. Chem. Lett.* **2013**, *4*, 2061−2068.
(13) Ellingson, R. J.; Beard, M. C.; Johnson, J. C.; Yu, P.; Micic, O. I.; Nozik, A. J.; Shabaev, A.; Efros, A. L. Highly Efficient Multiple Exciton Generation in Colloidal PbSe and PbS Quantum Dots. *Nano Lett.* **2005**, *5*, 865−871.
(14) Nootz, G.; Padilha, L. A.; Levina, L.; Sukhovatkin, V.; Webster, S.; Brzozowksi, L.; Sargent, E. H.; Hagan, D. J.; Stryland, E. W. V. Size Dependence of Carrier Dynamics and Carrier Multiplication in PbS Quantum Dots. *Phys. Rev. B* **2011**, *83*, 155302.
(15) Schaller, R. D.; Klimov, V. I. High Efficiency Carrier Multiplication in PbSe Nanocrystals: Implications for Solar Energy Conversion. *Phys. Rev. Lett.* **2004**, *92*, 186601.
(16) Beard, M. C.; Midgett, A. G.; Law, M.; Semonin, O. E.; Ellingson, R. J.; Nozik, A. J. Variations in the Quantum Efficiency of Multiple Exciton Generation for a Series of Chemically Treated PbSe Nanocrystal Films. *Nano Lett.* **2009**, *9*, 836−845.
(17) Semonin, O. E.; Luther, J. M.; Choi, S.; Chen, H.-Y.; Gao, J.; Nozik, A. J.; Beard, M. C. Peak External Photocurrent Quantum Efficiency Exceeding 100% via MEG in a Quantum Dot Solar Cell. *Science* **2011**, *334*, 1530−1533.
(18) Schaller, R. D.; Petruska, M. A.; Klimov, V. I. Effect of Electronic Structure on Carrier Multiplication Efficiency: Comparative Study of PbSe and CdSe Nanocrystals. *Appl. Phys. Lett.* **2005**, *87*, 253102.
(19) Schaller, R. D.; Pietryga, J. M.; Klimov, V. I. Carrier Multiplication in InAs Nanocrystal Quantum Dots with an Onset Defined by the Energy Conservation Limit. *Nano Lett* **2007**, *7*, 3469−3476.

(20) Beard, M. C.; Knutsen, K. P.; Yu, P.; Luther, J. M.; Song, Q.; Metzger, W. K.; Ellingson, R. J.; Nozik, A. J. Multiple Exciton Generation in Colloidal Silicon Nanocrystals. *Nano Lett.* **2007**, *7*, 2506−2512.
(21) Wang, S.; Khafizov, M.; Tu, X.; Zheng, M.; Krauss, T. D. Multiple Exciton Generation in Single-Walled Carbon Nanotubes. *Nano Lett.* **2010**, *10*, 2381−2386.
(22) Beard, M. C.; Luther, J. M.; Semonin, O. E.; Nozik, A. J. Third Generation Photovoltaics based on Multiple Exciton Generation in Quantum Confined Semiconductors. *Acc. Chem. Res.* **2012**, *46*, 1252−1260.
(23) Lin, Z.; Franceschetti, A.; Lusk, M. T. Size Dependence of the Multiple Exciton Generation Rate in CdSe Quantum Dots. *ACS Nano* **2011**, *4*, 2503−2511.
(24) Nozik, A. J. Multiple Exciton Generation in Semiconductor Quantum Dots. *Chem. Phys. Lett.* **2008**, *457*, 3−11.
(25) Schaller, R. D.; Sykora, M.; Pietryga, J. M.; Klimov, V. I. Seven Excitons at a Cost of One: Redefining the Limits for Conversion Efficiency of Photons into Charge Carriers. *Nano Lett.* **2006**, *6*, 424−429.
(26) McGuire, J. A.; Sykora, M.; Joo, J.; Pietryga, J. M.; Klimov, V. I. Apparent versus True Carrier Multiplication Yields in Semiconductor Nanocrystals. *Nano Lett.* **2010**, *10*, 2049−2057.
(27) Schaller, R. D.; Sykora, M.; Jeong, S.; Klimov, V. I. High-Efficiency Carrier Multiplication and Ultrafast Charge Separation in Semiconductor Nanocrystals Studied via Time-Resolved Photoluminescence. *J. Phys. Chem. B* **2006**, *110*, 25332−25338.
(28) Nair, G.; Bawendi, M. G. Carrier Multiplication Yields of CdSe and CdTe Nanocrystals by Transient Photoluminescence Spectroscopy. *Phys. Rev. B* **2007**, *76*, 081304.
(29) Nair, G.; Geyer, S. M.; Chang, L.-Y.; Bawendi, M. G. Carrier Multiplication Yields in PbS and PbSe Nanocrystals Measured by Transient Photoluminescence. *Phys. Rev. B* **2008**, *78*, 125325.
(30) Beard, M. C.; Midgett, A. G.; Hanna, M. C.; Luther, J. M.; Hughes, B. K.; Nozik, A. J. Comparing Multiple Exciton Generation in Quantum Dots to Impact Ionization in Bulk Semiconductors: Implications for Enhancement of Solar Energy Conversion. *Nano Lett.* **2010**, *10*, 3019−3027.
(31) Shabaev, A.; Efros, A. L.; Nozik, A. J. Multiexciton Generation by a Single Photon in Nanocrystals. *Nano Lett.* **2006**, *6*, 2856−2863.
(32) Allan, G.; Delerue, C. Role of Impact Ionization in Multiple Exciton Generation in PbSe Nanocrystals. *Phys. Rev. B* **2006**, *73*, 205423.
(33) Franceschetti, A.; An, J. M.; Zunger, A. Impact Ionization Can Explain Carrier Multiplication in PbSe Quantum Dots. *Nano Lett.* **2006**, *6*, 2191−2195.
(34) Sukhovatkin, V.; Hinds, S.; Brzozowski, L.; Sargent, E. H. Colloidal Quantum-Dot Photodetectors Exploiting Multiexciton Generation. *Science* **2009**, *324*, 1542−1544.
(35) Silvestri, L.; Agranovich, V. M. Direct Photogeneration of Biexcitons via Virtual Single-Exciton and Biexciton States in PbSe Quantum Dots. *Phys. Rev. B* **2010**, *81*, 205302.
(36) Stewart, J. T.; Padilha, L. A.; Qazilbash, M. M.; Pietryga, J. M.; Midgett, A. G.; Luther, J. M.; Beard, M. C.; Nozik, A. J.; Klimov, V. I. Comparison of Carrier Multiplication Yields in PbS and PbSe Nanocrystals: The Role of Competing Energy-Loss Processes. *Nano Lett.* **2012**, *12*, 622−628.
(37) Klimov, V. I. Spectral and Dynamical Properties of Multiexcitons in Semiconductor Nanocrystals. *Annu. Rev. Phys. Chem.* **2007**, *58*, 565−573.
(38) Tubtimtae, A.; Wu, K.-L.; Tung, H.-Y.; Lee, M.-W.; Wang, G. J. Ag_2S Quantum Dot-Sensitized Solar Cells. *Electrochem. Commun.* **2010**, *12*, 1158−1160.
(39) Xie, Y.; Yoo, S. H.; Chen, C.; Cho, S. O. Ag_2S Quantum Dots-Sensitized TiO_2 Nanotube Array Photoelectrodes. *Mater. Sci. Eng., B* **2012**, *177*, 106−111.
(40) Yang, H.-Y.; Zhao, Y.-W.; Zhang, Z.-Y.; Xiong, H.-M.; Yu, S.-N. One-Pot Synthesis of Water-Dispersible Ag_2S Quantum Dots with Bright Fluorescent Emission in the Second Near-Infrared Window. *Nanotechnology* **2013**, *24*, 055706.
(41) Du, Y.; Xu, B.; Fu, T.; Cai, M.; Li, F.; Zhang, Y.; Wang, Q. Near-Infrared Photoluminescent Ag_2S Quantum Dots from a Single Source Precursor. *J. Am. Chem. Soc.* **2010**, *132*, 1470−1471.
(42) Hong, G.; Robinson, J. T.; Zhang, Y.; Diao, S.; Antaris, A. L.; Wang, Q.; Dai, H. In Vivo Fluorescence Imaging with Ag_2S Quantum Dots in the Second Near-Infrared Region. *Angew. Chem., Int. Ed.* **2012**, *51*, 9818−9821.
(43) Tang, J.; Sargent, E. H. Infrared Colloidal Quantum Dots for Photovoltaics: Fundamentals and Recent Progress. *Adv. Mater.* **2011**, *23*, 12−29.
(44) Klimov, V. I.; Mikhailovsky, A. A.; McBranch, D. W.; Leatherdale, C. A.; Bawendi, M. G. Quantization of Multiparticle Auger Rates in Semiconductor Quantum Dots. *Science* **2000**, *287*, 1011−1013.
(45) Kissel, H.; Müller, U.; Walther, C.; Masselink, W. T.; Mazur, Y. I.; Tarasov, G. G.; Lisitsa, M. P. Size Distribution in Self-Assembled InAs Quantum Dots on GaAs (001) for Intermediate InAs Coverage. *Phys. Rev. B* **2000**, *62*, 7213−7218.
(46) Nozik, A. J. Exciton Multiplication and Relaxation Dynamics in Quantum Dots: Applications to Ultrahigh-Efficiency Solar Photon Conversion. *Inorg. Chem* **2005**, *44*, 6893−6899.
(47) Tuan Trinh, M.; Houtepen, A. J.; Schins, J. M.; Hanrath, T.; Piris, J.; Knulst, W.; Goossens, A. P. L. M.; Siebbeles, L. D. A. In Spite of Recent Doubts Carrier Multiplication Does Occur in PbSe Nanocrystals. *Nano Lett.* **2008**, *8*, 1713−1718.
(48) Dvorak, M.; Wei, S.-H.; Wu, Z. Origin of the Variation of Exciton Binding Energy in Semiconductors. *Phys. Rev. Lett.* **2013**, *110*, 016402.
(49) Mohammed, O. F.; Adamczyk, K.; Banerji, N.; Dreyer, J.; Lang, B.; Nibbering, E. T. J.; Vauthey, E. Direct Femtosecond Observation of Tight and Loose Ion Pairs upon Photoinduced Bimolecular Electron Transfer. *Angew. Chem., Int. Ed.* **2008**, *47*, 9044−9048.
(50) Luther, J. M.; Beard, M. C.; Song, Q.; Law, M.; Ellingson, R. J.; Nozik, A. J. Multiple Exciton Generation in Films of Electronically Coupled PbSe Quantum Dots. *Nano Lett.* **2007**, *7*, 1779−1784.
(51) El-Ballouli, A. O.; Alarousu, E.; Usman, A.; Pan, J.; Bakr, O. M.; Mohammed, O. F. Real-Time Observation of Ultrafast Intraband Relaxation and Exciton Multiplication in PbS Quantum Dots. To be published.
(52) Sykora, M.; Petruska, M. A.; Alstrum-Acevedo, J.; Bezel, I.; Meyer, T. J.; Klimov, V. I. Photoinduced Charge Transfer between CdSe Nanocrystal Quantum Dots and Ru−Polypyridine Complexes. *J. Am. Chem. Soc.* **2006**, *128*, 9984−9985.
(53) Zidek, K.; Zheng, K.; Ponseca, C. S.; Messing, M. E.; Wallenberg, L. R.; Chabera, P.; Abdellah, M.; Sundstrom, V.; Pullerits, T. Electron Transfer in Quantum-Dot-Sensitized ZnO Nanowires: Ultrafast Time-Resolved Absorption and Terahertz Study. *J. Am. Chem. Soc.* **2012**, *134*, 12110−12117.
(54) Jiang, P.; Zhu, C.-N.; Zhang, Z.-L.; Tian, Z.-Q.; Pang, D.-W. Water-Soluble Ag_2S Quantum Dots for Near-Infrared Fluorescence Imaging In Vivo. *Biomaterials* **2012**, *33*, 5130−5135.